Articles

Polymer Core−Shell Fibers with Metal Nanoparticles as Nanoreactor for Catalysis

Martin Graeser,*,† Eckhard Pippel‡, Andreas Greiner†, and Joachim H. Wendorff†

Center of Material Science, Philipps-University, Marburg 35032, Germany, and Max-Planck-Institute of Microstructure Physics, Weinberg 2, 06120 Halle, Germany

Received April 17, 2007; Revised Manuscript Received June 16, 2007

ABSTRACT: We have prepared polymer core−shell fibers containing salts of palladium, rhodium, and platinum. These salts were reduced within the core of the fibers by thermal decomposition at elevated temperatures and by using hydrogen as reduction medium. Monometal nanoparticles as well as mixed bimetal nanoparticles were produced in this way. The resulting fibers consisted either of a hollow core carrying the nanoparticles or a polymer core in which the nanoparticles were distributed. Both systems were successfully applied to specific hydrogenation reactions in which the shell served the purpose of immobilizing the catalyst nanoparticles, controlling the access to them, and allowing their recovery after the reaction whereas the core acted as the confined reaction site with an easy access of the reactants to the catalytic sites.

Introduction

Metal nanoparticles display a huge potential in the area of heterogeneous catalysis for a number of reasons. A unique feature is that the catalytic activity strongly depends on the size.[1,2] The reduction in size down toward the several nanometers scale causes, first of all, modifications of their electronic structure; i.e., the Fermi energy is increased, causing a reduction of the redox potential. Furthermore, the surface morphology may change and thus the catalytic properties as the size is decreased. A reduction of the size may in addition cause modifications in the crystal structure of the metal.

Further effects arise as we go from single metal particles to bimetallic particles.[3−5] The limiting structures are the one where the two metals are mixed homogeneously within the nanoparticles and the other one where they are arranged as core and shell. The presence of the second metal within the nanoparticle in more or a less random fashion can affect the catalytic properties in several ways. It may be inert, causing just a dilution of the catalytically active metal atoms, or it may control the relative position of the active atoms in a specific way. Frequently, core−shell particles are formed, giving rise to so-called ligand effects arising from an exchange of electrons. Monometal and in particular bimetal nanoparticle catalysts thus display a broad spectrum of catalytic effects which make them objects of interest both in basic research and in chemical industry.

Yet frequently the handling of such nanoparticles for catalysis is a major problem. They tend to aggregate, and the recovery from the product of the catalytic processes is often difficult. One solution is to use support materials such as zeolites, aluminum oxide, tin oxide, graphite, etc., which provide a large specific surface area for the attachment of the nanoparticles. The close contact between the nanoparticles and the carrier material may however modify the catalytic properties such as the activity and the selectivity, both significant for monometal nanoparticles as well as bimetal nanoparticles.[1,5,6] Details of such effects depend on the electronic nature of the support medium be it a conductor, a semiconductor, or an insulator. Strong effects arise, for instance, in the case of graphite supports or TiO_2 supports, etc. Frequently, the catalytic activity is even strongly reduced in the presence of the support medium.

It seems that an approach based on support systems which will affect the electronic structure of the metal nanoparticles to a much lesser extent is a good choice in many cases. Micellar metal hybrid structures including polymer micelle metal hybrid structures where the metal nanoparticles are surrounded by polymer shells in the latter case is such an approach.[7−10] These shells reduce the tendency toward aggregation considerably and cause a high solubility of the particles in solution. Such catalytic hybrid systems thus combine in a certain sense homogeneous and heterogeneous catalytic effects.

The role of the shell may go well beyond the effects described above despite the rather weak particle−shell interactions. It has, for instance, been observed for complexes of metal nanoparticles with the polymer PVP (polyvinylpyrrolidone) that, in fact, the catalytic activity can be favorably modified in the sense that a catalytic system composed of the metal nanoparticle, the PVP shell, and chiral additives dissolved in the polymer complex may strongly enhance the stereoselectivity of the catalytic process.[11]

In addition, these micellar systems allow a recovery of the catalytic particles for instance by changing the solvent in such a way that a segregation of the nanoparticles takes place.[12] Catalyst recovery steps, based for instance on the induction of segregation of the particles in solution or the recovery based on superfiltration, are feasible yet require additional handling

* Corresponding author. E-mail: graeser@staff.uni-marburg.de.
† Philipps-University.
‡ Max-Planck-Institute of Microstructure Physics.

10.1021/ma070898d CCC: $37.00
Published on Web 07/26/2007

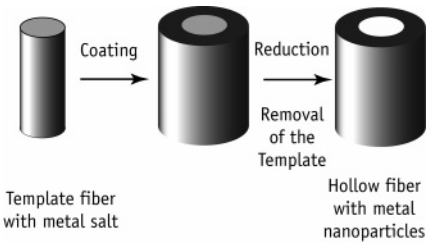

Figure 1. Core−shell nanoreactor concept with nanoparticles inside the tube.

process in batch reactions. Such types of recovery processes become unpractical as far as continuous processes are concerned as for instance in microreaction processing. In view of these results obtained for the micellar catalytic systems involving metal nanoparticles, it seems worthwhile to look for additional steps of optimizing such catalytic systems based on monometallic and in particular bimetallic nanoparticles both in terms of the catalytic properties and in terms of handling of recovery.

A first step consists in replacing the spherically shaped micellar shell of the catalytic metal nanoparticles by a support system having the shape of nanofibers. The actual concept which is described in this paper (Figure 1) goes beyond this support modification. It considers core−shell nanofibers assuming first of all the function of a confining nanoreactor for the preparation of the catalyst nanoparticles by transforming precursor salts for the single metallic or bimetallic nanoparticles into well-defined catalytic nanoparticles. Second, these core−shell nanofibers serve as confinement structure for the reaction which these nanoparticles catalyze. The core may be composed in addition to the nanoparticles of a solid or swollen polymer environment or a solvent acting as the reaction environment. In addition, the core may contribute further to the reaction by providing for instance chiral molecules.[11] The shell material also has a set of functions—one being the immobilization of the nanoparticle and their reactive environment and a second the selection of the species approaching the catalytic sites.

A typical setup would be an oriented nonwoven arrangement of such core−shell fibers stabilized by a more solid mesh through which the reactand mixtures—in the gaseous or fluid state—are pumped for instance in a microreaction setup (Figure 2).

This paper is concerned with the preparation of catalytic systems composed of core−shell nanofibers made from polymers. It reports on the use of such nanosystems as nanoreactors to control the formation of the nanoparticles in a highly defined way, and it reports on some catalytic model reactions involving the reduction of specific organic model compounds.

Experimental Section

Selection of Metals. The catalytic reaction which we have chosen as model reaction is the hydrogenation reaction. Metals such as palladium, rhodium, and platinum are good choices for such a reaction, and both monometal nanoparticles, but in particular bimetallic nanoparticles composed of them, seem to be highly promising in this respect. We selected the following metal salts as precursor materials to be incorporated into the core materials: palladium(II) acetate, chloro(1,5-cyclooctadiene)rhodium(I) dimer, rhodium(II) acetate, dichloro(1,5-cyclooctadiene)platinum(II), and platinum(II) acetylacetonate.

Polymer Materials. We used both an amorphous polylactide PDLLA (poly-DL-lactide, Resomer R 208, Boehringer Ingelheim) and a partially crystalline poly(ethylene oxide) (PEO, MW 900 000, Acros) as material for the production of the core fibers. Polylactide and poly(ethylene oxide) can be spun to core fibers from water and dichloromethane, respectively, and the fiber diameters can be

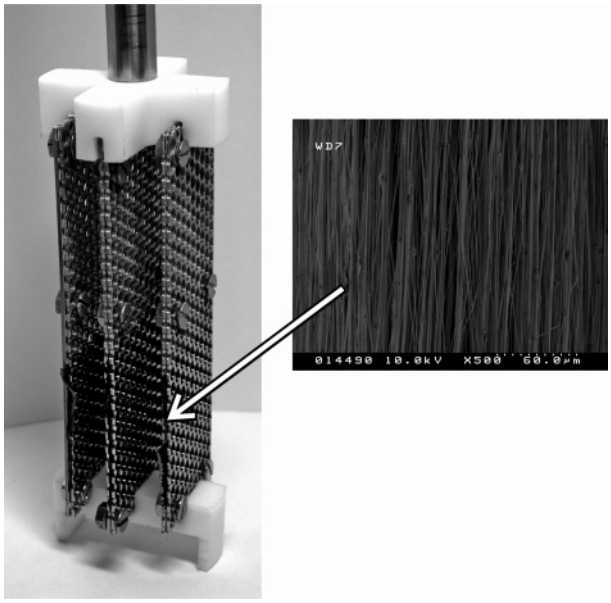

Figure 2. Architecture of the catalyst system.

controlled within a range of a few nanometers up to about 1 μm. Poly-*p*-xylylene (PPX) was chosen as shell material because of its low solubility and good permeation properties. It is stable in most solvents, and it can be deposited in a highly controlled way from the vapor phase which allows a perfect homogeneous coverage even for fibers with more complex topology such as porous fibers.[13,14]

Preparation of the Composite Core Fibers. The core fibers were prepared by electrospinning.[15−18] A polymer solution containing metal salts as precursor systems such as palladium acetate, chloro(1,5-cyclooctadiene)rhodium(I) dimer, or dichloro(1,5-cyclooctadiene)platinum(II) (see above) was pumped for this purpose from a reservoir through a die. An electric field of the order of a 2 kV/cm was applied to the die acting as one electrode and a counter electrode. The electric field causes charging of the drop emerging from the die and thus a deformation toward a conical shape and at higher fields the formation of a thin fluid jet starting at the tip of the deformed droplet. The volume elements within the jet are accelerated toward the counter electrode, and they are subjected during the process both to the evaporation of the solvent and to strong bend instabilities (whipping instabilities) which cause a strong stretching and thinning of the jet. A solidified composite nanofiber composed of the polymer and a homogeneous distribution of the metal salts are deposited on the counter electrode. The fiber diameters are of the order of some hundreds of nanometers, yet they can be controlled down to diameters of only a few nanometers.

The nanofibers carrying the precursor salts were subjected in the next step to the deposition of a polymer shell composed of poly-*p*-xylylene from the vapor phase.[13,14] The precursor [2.2]-paracyclophane was heated up for this purpose to 650 °C to initiate the decomposition of the precursor to reactive species which are deposited at very moderate temperatures of about 30 °C onto the fiber to form the polymer layer. Independent studies have revealed that such films are pinhole-free for a layer thickness larger than 500 nm. In this way core−shell polymer fibers result in which tiny precursor salt crystals are homogeneously distributed within the core (see below).

Formation of Nanoparticles from the Salts. Various approaches have been tested toward the formation of nanoparticles both from single metals and for bimetal systems. We will not consider the milling approach here starting from macroscopical particles but rather approaches based on precursor salts. Possible approaches involve the alcohol reduction approach, electrochemical methods, photoreduction,[19,20] sonochemical methods, or microwave-based approaches to name just a few.[21] We have decided to use the thermal decomposition approach in the absence or presence of hydrogen. Again different routes are available in this case as far as bimetal

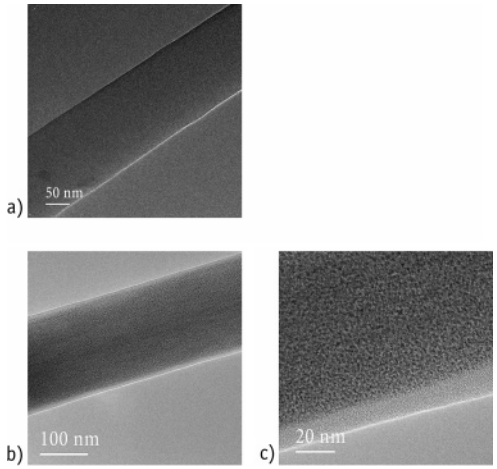

Figure 3. Polylactide nanofibers obtained via electrospinning without (a) and with metal salts (b, c).

nanoparticles are the goal. We might choose the use of zwitter salts containing both types of metals, the reduction of one metal salt in the presence of nanoparticles of the second metal, previously obtained by reduction, or the reduction of mixtures of the salts each containing one particular metal.

We have chosen the last approach mentioned since it seems to be the most flexible way. We used both a thermally induced reaction approach and an approach using hydrogen as reducing agent. The temperature amounts in the first case to about 230 °C for the case of polylactide as core material and to about 130 °C if the reduction is performed in the presence of hydrogen (see below).

Results and Discussion

Nanofibers with Metal Salts. Electrospinning was used to prepare polymer nanofibers containing the metal precursor salts. We used both the amorphous polylactide PDLLA and the partially crystalline poly(ethylene oxide) as polymer carrier for the precursor salts, the solvent being dichloromethane. Experimental details are given above. The precursor salts were added to the spinning solution. Polymer/salt concentrations were chosen in the weight ratios of 1:1, 2:1, and 4:1, respectively. The polymer concentration relative to the solvents were in the range of 4 and 2.7 wt % for PDLLA and PEO, respectively.

Electrospinning gave in all cases rise to well-defined nanofibers with diameters ranging from about 200 to 600 nm. In principle, we have shown that we are able to control the fiber diameter for these polymers in the range between a few

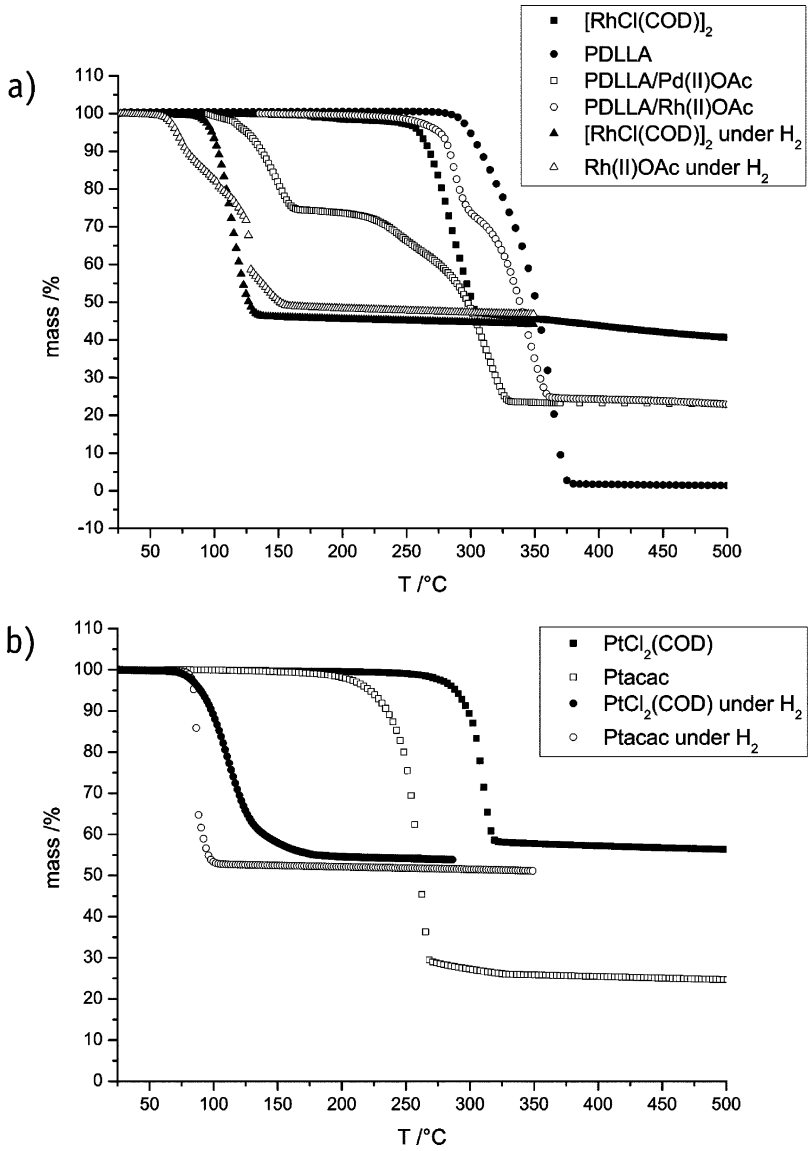

Figure 4. TGA diagrams obtained for the polymer PDLLA and the metal salts distributed within the polymer: (a) for rhodium and palladium salts and (b) for platinum salts.

nanometers and about 1 μm in a highly defined way by choosing the spinning parameters appropriately. Yet for the purpose of using the fibers for catalysis and in view of the mechanical forces to which the fibers will be subjected in flow through arrangements, a diameter in the range of a few hundred nanometers is advisable.

Electron microscopical investigations on fibers both without salts and with salts included showed smooth fibers without the presence of beads or pores (Figure 3a,b). Fiber formation is known to happen very rapidly, the take-up speed amounting to 37 m/s in our case. Fibers are theoretically infinitely long. Theoretical estimates predict a characteristic structure formation time of a few milliseconds. So the expectation might be that the salts are homogeneously dispersed within the fibers in a similar way as in the starting solutions.

A closer inspection of the electron microscopical diagrams (Figure 3c) reveals, however, that the metal salts form very tiny crystals with a diameter of about 1.5 nm. It thus seems that crystal nucleation has already taken place during the rapid structure formation process of the nanofiber, yet the growth of the crystals was frozen-in due to the solidification of the fibers originating from the evaporation of the solvents leading to a glass formation or a crystal growth. These metal salt crystals will to a certain extent control the size of the nanocrystals which will grow from the salts.

Thermal Decomposition of the Metal Salts. We used different approaches toward reducing the metal salts to metal nanoparticles, as already discussed in the experimental part: thermal decomposition in the presence of nitrogen or vacuum as well as the reduction in the presence of hydrogen. Here we consider the thermal stability both of the polymer used and of the metal salts employing TGA (thermogravimetric analysis). The polylactide which can be expected to contribute to the reduction process is found to start to decompose in the presence of nitrogen at about 280 °C, and the decomposition is complete at about 375 °C as apparent from the TGA curves displayed in Figure 4.

The palladium acetate begins to decompose already at a temperature of about 100 °C, and the decomposition is complete at about 160 °C, as is obvious from Figure 4a. The metal content of the salt amounts to about 48 wt % so that the final mass of the metal nanoparticles within the fibers amounts to about 25%, as is also obvious from the TGA diagram. The polymer itself is decomposed in a second step at much higher temperatures. The decomposition of the rhodium acetate takes place in a significantly higher temperature range as compared to the palladium salt. The TGA reveals a stepwise decrease of the total mass of the metal salt containing PDLLA fibers starting at about 245 °C and ending at about 300 °C. It is in this temperature range that a second stepwise decrease of the mass takes place due to the decomposition of the polymer fibers. We found that the decomposition of the rhodium acetate happens at slightly lower temperatures if the decomposition is done in vacuum. The platinum salts (Figure 4b) decompose in the temperature range between 250 and about 300 °C. From the low residue percentage of Ptacac it can be seen that this salt partly sublimates.

Formation of the Monometal Nanoparticles. To start with, we will discuss the formation of metal nanoparticles composed of just one metal. The thermal decomposition of the palladium acetate and of the rhodium acetate in the presence of nitrogen has already been discussed above. The results of the decomposition in both cases are metal nanoparticles with diameters in the range of 5−10 nm. Parts a and b of Figure 5 reveal these

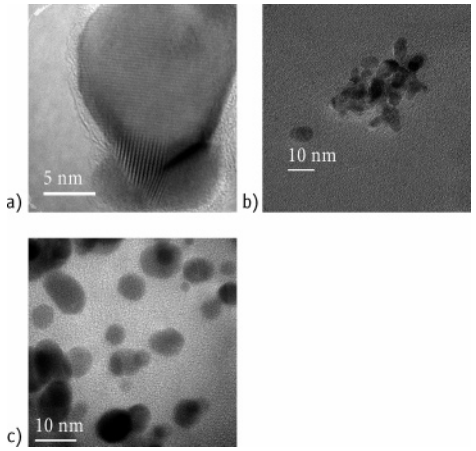

Figure 5. Metal particles obtained by thermal decomposition: (a) palladium, (b) rhodium, and (c) platinum.

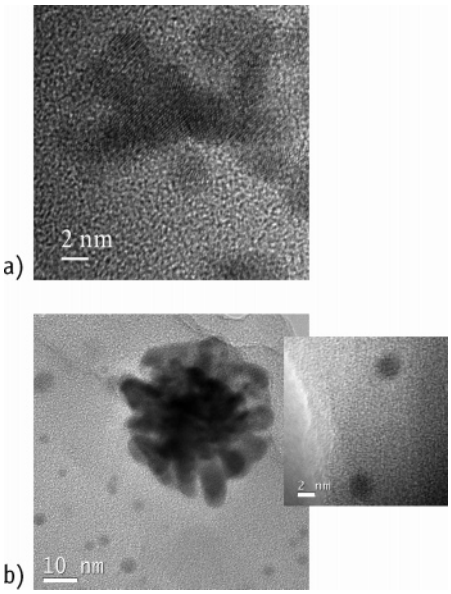

Figure 6. Metal particles obtained by hydrogen reduction: (a) rhodium and (b) platinum.

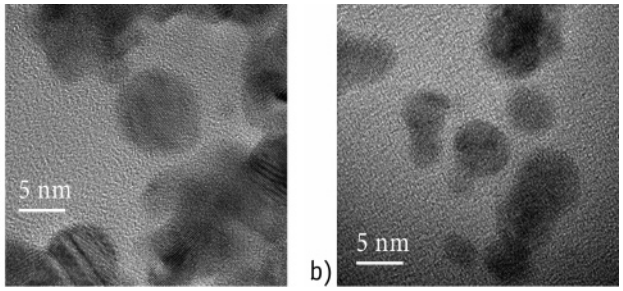

Figure 7. Bimetallic nanoparticles of palladium/rhodium: (a) thermal decomposition and (b) hydrogen reduction.

nanoparticles for the case of palladium and rhodium, respectively. The shapes are not really spherical but rather seem to be controlled by particular lattice planes defining the contour. The shown figures present the nanoparticles after removing the polymer matrix which they had been distributed nearly homogeneously in. The nanoparticles tend to aggregate in different fashions depending on the nature of the nanoparticles.

Hydrogen Reduction of Metal Salts. Next, the results obtained from the reduction of the metal salts in the presence of hydrogen will be considered. In this case the reduction took place at a much lower temperature starting at about 70 °C as

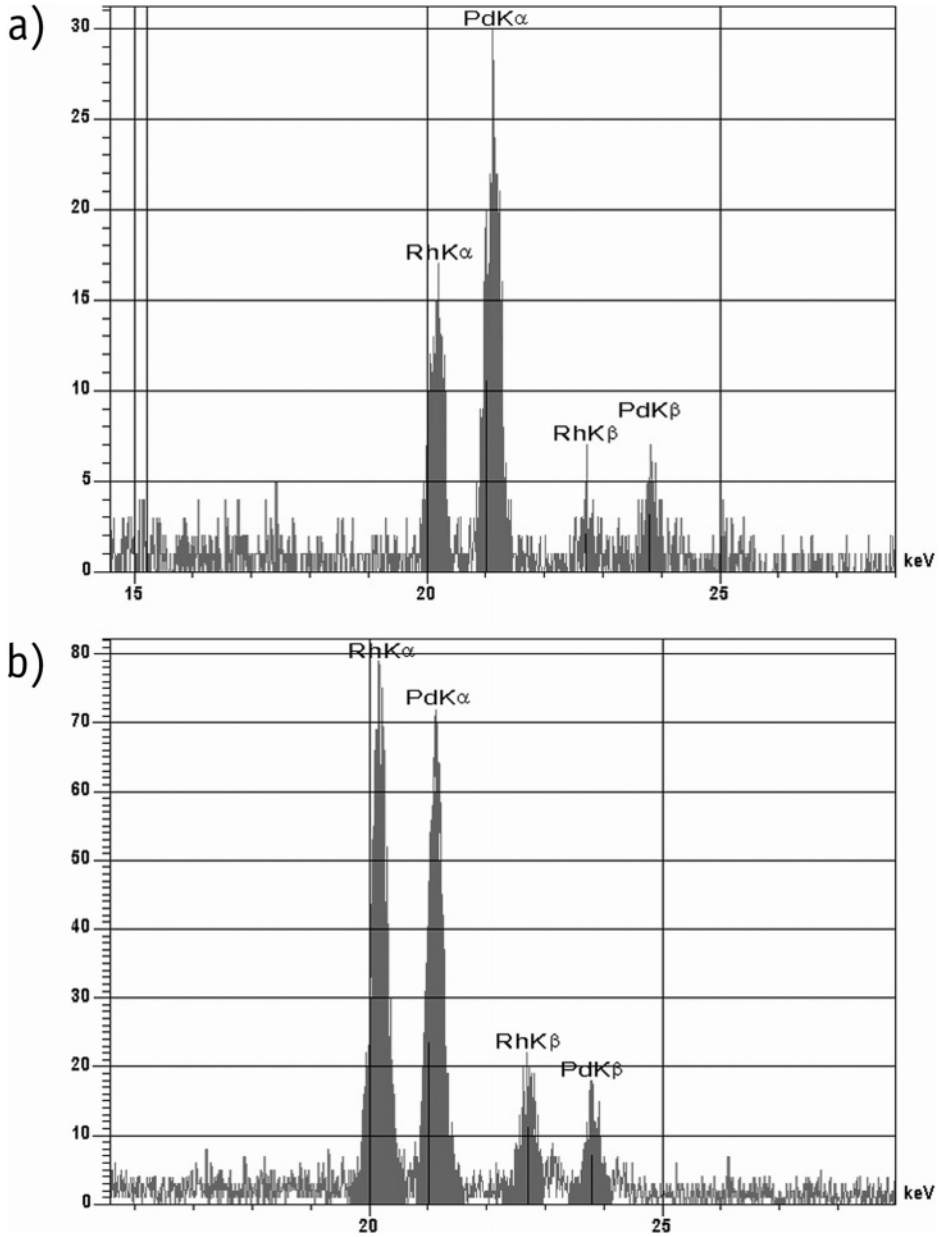

Figure 8. EDX analysis of the rhodium/palladium nanoparticles: (a) thermal decomposition and (b) hydrogen reduction.

compared to 230 °C used for the thermal decomposition. Figure 6a,b reveals the sizes and shapes of the resulting metal nanoparticles. It is obvious from these figures that in general the size and the shape of the nanoparticles are not too different from the ones obtained by thermal decomposition as far as the rhodium particles are concerned. It thus seems that coarsening effects do not play a role even at elevated temperatures. In fact, annealing studies taking place at an annealing temperature of 230 °C for an annealing period of 48 h also did not give indications on coarsening.

A peculiar feature was observed for the reduction of the platinum nanoparticles. We observed the formation of well-defined aggregates with a somewhat star-shaped appearance having a diameter in the range between 50 and 100 nm being composed of individual nanoparticles in the 5−10 nm scale. In addition, we found individual platinum nanoparticles with diameters as small as 2 nm.

Formation of Bimetallic Nanoparticles. To obtain bimetallic nanoparticles, we started from PDLLA containing two different salts carrying the two metals we would like to combine within one nanoparticle. We restricted the relative concentration of the salts to a 1:1 mixture for these investigations. Again we have performed a thermal decomposition of the metal salts within the same temperature range as used for the preparation of the monometal nanoparticles, and we considered a reduction in the presence of hydrogen. The results are shown in Figure 7a,b for the case of palladium/rhodium nanoparticles. The size and the shape of the nanoparticles are very similar in both cases, and

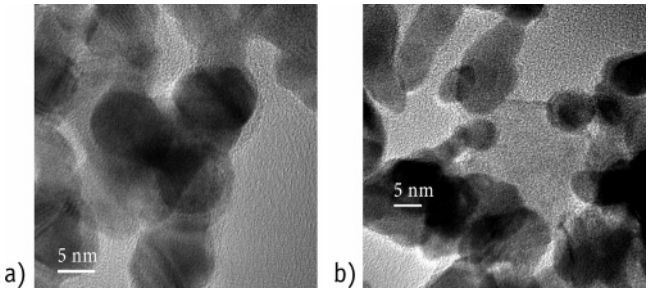

Figure 9. Palladium/platinum nanoparticles: (a) thermal decomposition and (b) hydrogen reduction.

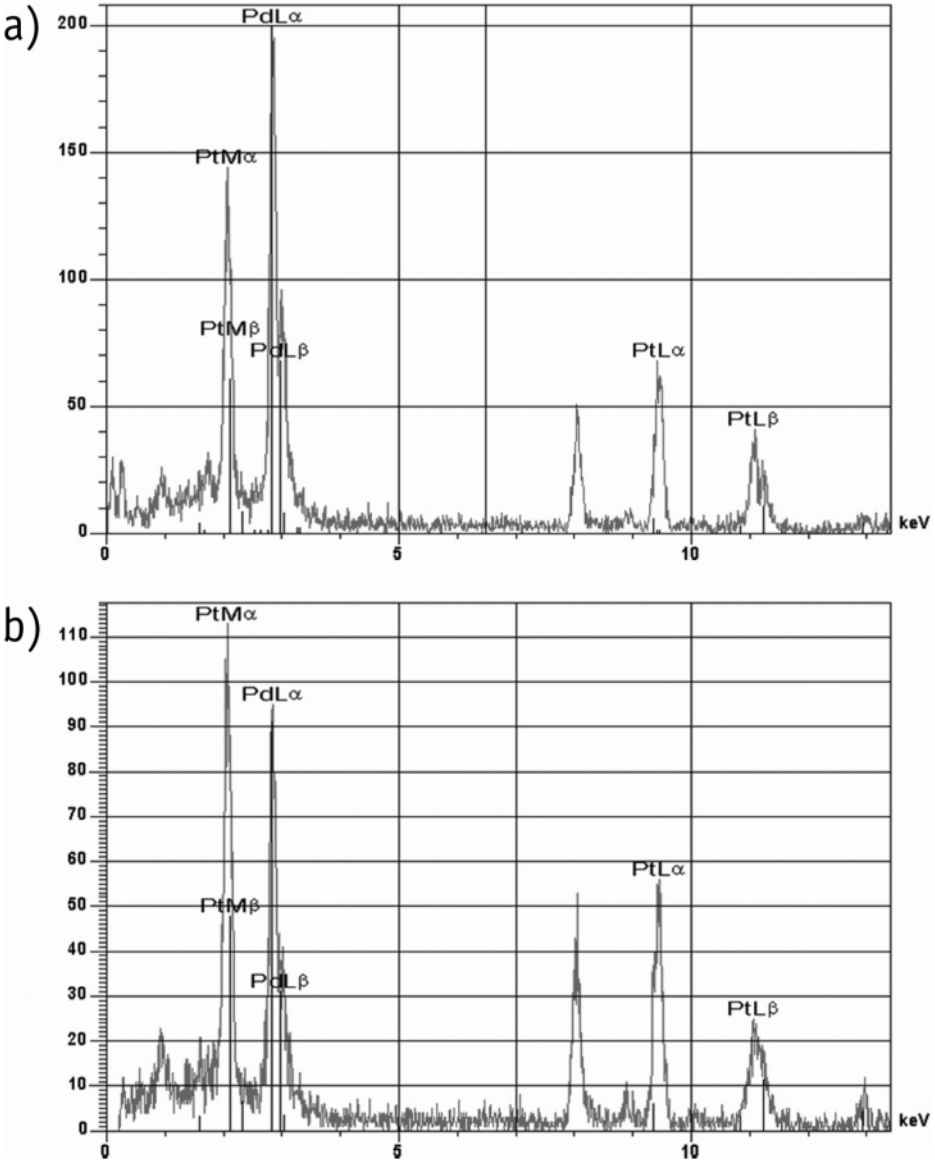

Figure 10. EDX analysis of the palladium/platinum nanoparticles: (a) thermal decomposition and (b) hydrogen reduction.

they agree with the sizes and shapes found for the monometallic nanoparticles.

To find out whether the two atoms are really incorporated within one and the same nanoparticle, we operated the transmission electron microscope in the scanning transmission microscope mode with a beam diameter of 2 nm, and we performed an EDX analysis. The average results obtained for single nanoparticles are displayed in Figure 8 for both types of reduction of the metal salts with composition deviations among several particles of up to 5% only. It is obvious that the nanoparticle contains both types of metal atoms, yet it is also obvious that the composition depends on the route used for the reduction. The nanoparticles obtained via hydrogen reduction consistently show a 1:1 composition as expected from the composition of the salt mixture. The rhodium concentration is strongly reduced if the thermal decomposition route is applied. It is down to about 25%. We will discuss this result later after having considered the results for the formation of the palladium/platinum nanoparticles.

For these nanoparticles we obtain very similar results both in terms of the size and shapes of the bimetallic nanoparticles and with respect to the compositions. The bimetallic particles obtained by hydrogen reduction are strongly elongated. These results are displayed in Figures 9 and 10, respectively.

Again the composition of the nanoparticles is 1:1 for the reduction in the presence of hydrogen, and it amounts to about 25% for the platinum if the thermal decomposition approach is used. We tentatively conclude that perhaps the rhodium and the platinum salts have evaporated before the decomposition took place, yet the TGA curves do not give any indications for such an effect. Thermal decomposition in vacuum and in the presence of argon do not give different results. So this is still an open problem.

In principle, we expect two limiting structures for nanoparticles composed of two metals: a homogeneous mixture within the nanoparticle or a core−shell nanoparticle (Figure 11). The actual structure that will form is strongly controlled by the redox potential of the metals used for nanoparticle formation. The metal with the strongest redox potential will form the core structure as the reduction takes on which the metal with the lower redox potential will be deposited in the later stage of the reduction of the salt mixture. So in the cases considered here

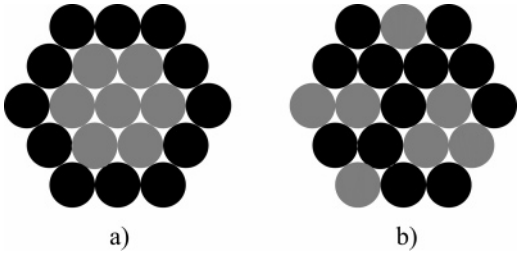

Figure 11. Core−shell structure (a) and homogeneous mixture (b).

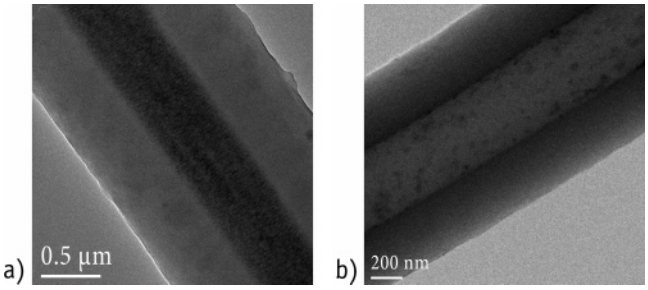

Figure 12. Catalyst system: (a) coated electrospun PEO fiber with metal nanoparticles after hydrogen reduction; (b) after solvent extraction of the PEO core.

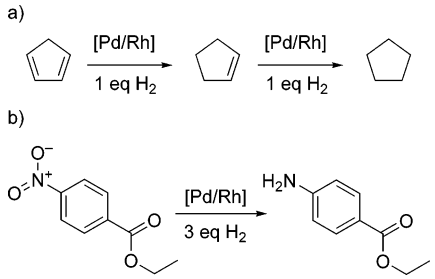

Figure 13. Model reactions.

the tendency to form the core increases in the sequence Pt > Pd > Rh following the sequence of redox potentials, but it also depends on the order of reduction of the salts.

What is known in any case is that on a macroscopical scale in bulk material a broad range of compositions between these metals is not accessible; the corresponding compositions will phase separate, opening a nonaccessible composition range extending for instance from a few wt % of the one component to a few wt % of the other component.[22−24] This situation is quite different in particles on the nanoscale due to modified internal structures and surface properties The compositions that we observe within the nanoparticles are well within the macroscopically nonaccessible range.

Catalysis. Model Reactions. We used the core−shell polymer fibers shown in Figure 12 with the bimetal nanoparticles of palladium and rhodium dispersed in them for the model hydrogenation reactions displayed in Figure 13. The reactions were performed in solution using ethanol as the reaction solvent. The metal nanoparticles within the core are thus surrounded either by the reactants and the solvent permeating through the wall material or in addition by a swollen polymer. It will become obvious below that the presence of the swollen polymer may control the reaction speed. The oriented fibers were stabilized by a solid stainless steel mesh (see Figure 2) in an autoclave. During the reaction the reactand solution was stirred to achieve a constant flow through the fiber web.

The two model reactions shown in Figure 13 have been used for testing of the catalyst system. All reactions were performed at room temperature. Reaction a was mentioned before for Pd/Rh nanoparticles incorporated in micelles to lead to a single hydrogenation step which would lead to cyclopentene.[25,26] In contradiction, the experiments with our catalyst system doubled the hydrogen uptake and lead directly to the completely hydrogenated cyclopentane. Although the second step took longer, this gives rise to a very active catalyst system.

The second reaction is a good test model due to different functional groups.[27,28] Usually Pd on charcoal is used in laboratory dimensions whereas industry uses a two-step pathway for this special product which is used in pharmacy. Our catalyst system leads with 100% conversion to the amine. No side products or any starting material could be detected by gas chromatography. The catalyst holder was taken out of the solution, and the latter was evaporated to give the pure product. No purification was necessary. The catalyst holder was spilled with some ethanol and could be reused at once. Several subsequent uses did not show any loss in catalyst activity. No change in catalyst activity occurred after several reaction cycles, and no alteration in fiber morphology was recognizable in TEM.

In the case of the catalyst system without removal of the core fiber the reaction duration doubled, but there was no change in result of the product.

The experiments of reaction b were repeated with Pd on charcoal with the same overall load of metal and appeared to be only slightly faster. But considering that there is an additional filtration step to remove the catalyst, the amount of time needed is higher, and cleaning of the catalyst for reuse takes longer and involves a higher consumption of solvent.

By reducing the thickness of the PPX coating or increasing the metal load of the fibers, a reduction of time should be possible.

Conclusions

A new way of in situ preparing ultrafine nearly monodispersed mono- and bimetallic nanoparticles has been developed. The resulting Pd−Rh particles have been incorporated into polymer nanotubes during formation to form a new catalyst system which has shown its high activity in hydrogenation reductions. The ease of removing and reusing it makes this bimetallic−polymer support a very promising catalyst system.

References and Notes

(1) Coq, B.; Figueras, F. In *Catalysis and Electrocatalysis at Nanoparticle Surfaces*; Wieckowski, A., Savinova, E. R., Vayenas, C. G., Eds.; Dekker: New York, 2003; pp 847−875.
(2) Niu, Y. H.; Yeung, L. K.; Crooks, R. M. *J. Am. Chem. Soc.* **2001**, *123*, 6840−6846.
(3) Toshima, N.; Yonezawa, T. *New J. Chem.* **1998**, *22*, 1179−1201.
(4) Teranishi, T.; Toshima, N. In *Catalysis and Electrocatalysis at Nanoparticle Surfaces*; Wieckowski, A., Savinova, E. R., Vayenas, C. G., Eds.; Dekker: New York, 2003; pp 379−407.
(5) Alexeev, O. S.; Gates, B. C. *Ind. Eng. Chem. Res.* **2003**, *42*, 1571−1587.
(6) Verykios, X. E. In *Catalysis and Electrocatalysis at Nanoparticle Surfaces*; Wieckowski, A., Savinova, E. R., Vayenas, C. G., Eds.; Dekker: New York, 2003; pp 745−783.
(7) Bönnemann, H.; Richards, R. M. *Eur. J. Inorg. Chem.* **2001**, 2455−2480.
(8) Teranishi, T.; Hosoe, M.; Tanaka, T.; Miyake, M. *J. Phys. Chem. B* **1999**, *103*, 3818−3827.
(9) Lee, C. L.; Wan, C. C.; Wang, Y. Y. *Adv. Funct. Mater.* **2001**, *11*, 344−347.
(10) Chung, Y. M.; Rhee, H. K. *Catal. Lett.* **2003**, *85*, 159−164.
(11) Zuo, X.; Liu, H.; Liu, M. *Tetrahedron Lett.* **1998**, *39*, 1941.
(12) Crooks, R. M.; Zhao, M. Q.; Sun, L.; Chechik, V.; Yeung, L. K. *Acc. Chem. Res.* **2001**, *34*, 181−190.

(13) Bognitzki, M.; Hou, H. Q.; Ishaque, M.; Frese, T.; Hellwig, M.; Schwarte, C.; Schaper, A.; Wendorff, J. H.; Greiner, A. *Adv. Mater.* **2000**, *12*, 637.
(14) Hou, H. Q.; Jun, Z.; Reuning, A.; Schaper, A.; Wendorff, J. H.; Greiner, A. *Macromolecules* **2002**, *35*, 2429−2431.
(15) Huang, Z. M.; Zhang, Y. Z.; Kotaki, M.; Ramakrishna, S. *Compos. Sci. Technol.* **2003**, *63*, 2223.
(16) Xia, Y.; Li, D. *Adv. Mater.* **2004**, *16*, 1151.
(17) Bognitzki, M.; Czado, W.; Frese, T.; Schaper, A.; Hellwig, M.; Steinhart, M.; Greiner, A.; Wendorff, J. H. *Adv. Mater.* **2001**, *13*, 70.
(18) Deitzel, J. M.; Kleinmeyer, J. D.; Hirvonen, J. K.; Beck, Tan, N. C. *Polymer* **2001**, *42*, 8163.
(19) Zhang, Z. Y.; Esrom, H.; Boyd, I. W. *Appl. Surf. Sci.* **1996**, *96*−*8*, 399.
(20) Fukuoka, A.; Araki, H.; Sakamoto, Y.; Inagaki, S.; Fukushima, Y.; Ichikawa, M. *Inorg. Chim. Acta* **2003**, *350*, 371.
(21) Dhas, N. A.; Gedanken, A. *J. Mater. Chem.* **1998**, *8*, 445.
(22) Tripathi, S. N.; Bharadwaj, S. R. *J. Phase Equilib.* **1994**, *15*, 208.
(23) Wang, Y.; Faulkner, J. S.; Stocks, G. M. *Phys. Rev. Lett.* **1993**, *70*, 3287.
(24) Guerler, R.; Cornish, L. A.; Pratt, J. N. *J. Alloys Compd.* **1993**, *191*, 165.
(25) Zhao, B.; Toshima, N. *Chem. Express* **1990**, *5*, 721−4.
(26) Chung, Y. M.; Rhee, H. K. *J. Mol. Catal. A: Chem.* **2003**, *206*, 291−298.
(27) Blaser, H. U.; Malan, C.; Pugin, B.; Spindler, F.; Steiner, H.; Studer, M. *Adv. Synth. Catal.* **2003**, *345*, 103−151.
(28) Studer, M.; Blaser, H. U.; Exner, C. *Adv. Synth. Catal.* **2003**, *345*, 45−65.

MA070898D